10.1109/ULTSYM.2013.0023

Ultrasonic attenuation imaging in a rodent thyroid cancer model

Omar Zenteno[1], William Ridgway[2], Sandhya Sarwate[2], Michael Oelze[2] and Roberto Lavarello[1]
[1]Laboratorio de Imágenes Médicas, Departamento de Ingeniería
Pontificia Universidad Católica del Perú, San Miguel, Lima 32, Perú.
[2] Bioacoustics Research Laboratory, Department of Electrical and Computer Engineering
University of Illinois at Urbana-Champaign, Urbana, IL 61801, USA.

***Abstract*—The incidence of diagnosed thyroid cancer has increased significantly over the last decades. Although advances in ultrasonic imaging have increased the malignancy detection rate, current ultrasonic imaging markers do not provide a sufficient level of diagnostic accuracy to replace biopsy. Recent studies suggest that ultrasound parameters derived from backscatter coefficients may allow differentiating among different types of thyroid tumors and normal tissues in a rodent model *ex vivo*. In this work, the potential use of attenuation coefficient (AC) estimates for the same purpose was explored. A sample set of 24 excised mice thyroids were scanned using a 40-MHz, f/3 single element transducer. The experimental dataset contained six animals that developed papillary thyroid carcinoma (PTC), five that developed follicular variant papillary thyroid carcinoma (FV-PTC), five that developed c-Cell adenoma (c-Cell) and eight that did not develop thyroid abnormalities (control). AC slope maps were generated with a spectral log difference method using 0.5mm by 0.5mm data blocks. Outliers of each slice due to artifacts in AC estimation were discarded using the Thompson Tau method. Finally, a Kruskal-Wallis test was conducted to analyze if statistically significant differences in the mean AC slope among the four groups existed. The median and interquartile range for each group were 1.29 and 0.22 dB/cm-MHz for the control group, 1.64 and 0.09 dB/cm-MHz for c-Cell, 1.16 and 0.12 dB/cm-MHz for PTC and 1.33 and 0.08 dB/cm-MHz for FV-PTC, respectively. These values are consistent with previous reports of attenuation in thyroid tissues. The Kruskal-Wallis test reported statistically significant differences between the c-Cell group and the other groups of study and between the PTC and FV-PTC groups ($p<0.05$). These preliminary results suggest that the AC may be used to characterize thyroid tissues.**

Keywords—Attenuation imaging, Tissue characterization, Thyroid cancer

I. INTRODUCTION

Thyroid cancer incidence rate has increased dramatically over the last decades due to improved detection. Estimates for the United States, Canada, Australia and Western Europe placed the annual rate of increase at 3% [1]. Moreover, 90% of this increment was due to the diagnosis of small papillary cancers and its variants [2].

Advances in imaging diagnostic techniques have increased the malignancy detection rate from this subclinical reservoir. While common thyroid ultrasound cannot diagnose all thyroid nodules, it can detect nodules as small as 2 mm, which is much more sensitive than physical examination alone (i.e., typical detected nodules >10 mm) [2]. However, it does not provide a sufficient level of accuracy in order to replace the fine needle aspiration (FNA) biopsy, which remains as the most accurate and sensitive test for the thyroid malignancy diagnosis.

Medical practice tends to prioritize patients health and most of the time asymptomatic benign tumors are being detected and treated as malignant. This leads to unnecessary surgery, which potentially has personal and societal consequences (e.g., the need of lifelong thyroid hormone replacement for patients and expenses to public health services) [3].

Recent studies suggest that quantitative ultrasound parameters (i.e., the effective scattering diameter (ESD) and the effective acoustic concentration (EAC)) have the potential to reduce unnecessary treatment by discriminating between cancerous and normal thyroids. However, in a study of quantitative ultrasound to differentiate thyroid cancer from normal and benign thyroid hyperplasias in mouse models, no parameter was able to differentiate the benign C-cell adenomas from the normal thyroids [4].

The present study complements these findings with quantitative ultrasound attenuation estimates using an analytical diffraction compensation function for the first time on the same three specific groups of oncogene mutations.

II. METHODS

A. Animal models and data adquisition:

The animal models consisted of mice that had introduced a dominant negative mutant thyroid nuclear receptor gene. As a result of this, many developed variations of papillary metastatic thyroid tumors or presented a high concentration of parafollicular cells (c-Cells) which are known to potentially lead to medullary carcinoma. When the thyroid appeared to have lesions or showed signs of hyperplasia, both thyroid lobes were extracted with a portion of the trachea and placed in a tank of degased 0.9% saline for ultrasonic scanning.

A sample set of 24 transgenic mice thyroids was scanned using a 40-MHz weakly-focused (f/3) single element transducer using a Olympus Panametrics 5900 pulser/receiver (Olympus NDT, Waltham, MA) for excitation. The radiofrequency (RF) data was captured by a PC using a 14-bit

UF3-4121 A/D card with 250 MHz sampling frequency (Strategic Test Corporation, Woburn, MA).

Each thyroid sample was scanned using a micro-positioning system controlled by custom LabVIEW (National Instruments, Austin, TX) software. Several slices were taken at 0.2-0.4 mm apart across the thyroid sample from the top view. The slices which fully contained both thyroid lobes were selected resulting in an average of six usable ultrasound slices per rodent. Each scan line within a slice had a separation of 50 μm. After scanning, each sample was excised, formalin-fixed and paraffin-embedded for histologic evaluation by light microscopy.

The histopathological classification reported that the sample was conformed of six papillary thyroid carcinoma (PTC), five follicular variant pattern papillary carcinoma (FV-PTC), five c-Cell positives (c-Cell) and eight mice which did not develop thyroid nodules. The latter were labeled as normal and used as control group.

B. Quantitative ultrasound attenuation coefficient (QUSAC):

Common B-mode ultrasound imaging has been the first hand diagnosis tool on soft tissue pathologies for several years due to its low cost and portability. However, diagnostics from conventional ultrasound are always subjective and heavily dependent on the operator's experience, medical training and image quality. On the other hand, QUSAC estimates offer numerical reliable depth- and frequency-dependent values based on the power spectrum of the RF data. The use of these parameters in medical practice can potentially reduce the diagnosis inter-operator variability and increase its efficiency.

Different attenuation estimation algorithms in the frequency domain have been reviewed in the literature (e.g., spectral and spectral log difference [5], hybrid method [5,6], spectral cross correlation [7], among others.) However, due to diffraction effects, the spectral properties of the signal are distorted and must be compensated by a frequency- and depth-dependent factor. The majority of the previously mentioned algorithms make use of a reference phantom with known attenuation coefficient to deal with these losses. In contrast, we present an analytical method based on Chen's method for backscatter coefficient estimation with single-element focused transducers [8,9].

C. Analytic attenuation estimation method:

The spectral information of the radiofrequency (RF) data from the image slices was processed to generate attenuation maps with a spectral log difference variant on custom MATLAB (MathWorks, Natick, MA) software.

The algorithm used the analytical backscatter coefficient (BSC) diffraction compensation function for single-element transducers proposed by Chen et al. [8], i.e.,

$$D_s(\bar{r},\omega) \cong \begin{cases} 0.46\cdot\frac{\pi a^2}{\bar{r}^2}\exp\left[\frac{-0.46}{\pi}\cdot G_p^2\cdot\left(\frac{f_l}{\bar{r}}-1\right)^2\right], & \left(\frac{1+\pi}{G_p}\right)^{-1} < \frac{\bar{r}}{f_l} < \left(\frac{1-\pi}{G_p}\right)^{-1} \\ \frac{\pi a^2}{\bar{r}^2}\cdot 1.07\cdot\left[G_p\cdot\left(\frac{f_l}{\bar{r}}-1\right)\right]^{-2}, & \text{otherwise,} \end{cases} \quad (1)$$

where G_p is the transducer pressure gain factor, $\bar{r}$ the distance from the transducer to the sample, a the transducer radius and f_l the focal length of the transducer.

The advantage of this approach is to avoid the need of a tissue mimicking reference phantom for system calibration and diffraction correction, which is problematic to construct at high frequencies. Although the formulation of Chen's model provides a reference power spectrum calculated using an acoustical mirror on the focal plane, the use of two different depth analysis regions removes the reference data dependent terms requirement.

A region of interest was outlined in the thyroid and data blocks of 0.6mm by 0.6mm with an 87.5% overlap in both directions were used to window data. Each group of lines inside a data block is divided into two shorter blocks, proximal and distal, determined by the size of the gating function as observed on Fig. 1. For each block, a Tukey window with α= 0.25 was used as gating function.

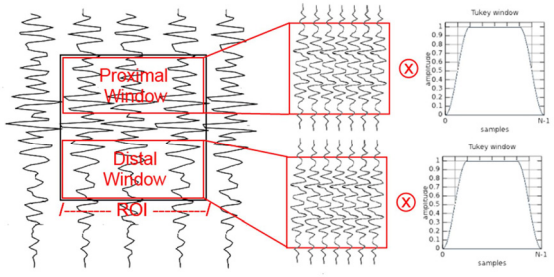

Fig. 1. Data block and gate function distribution over the sample. Data blocks were overlaid to increase spatial resolution of the attenuation maps.

The power spectrum of the ultrasound data received from a region centered at depth $\bar{r}$ is given by

$$\langle|V_s(\bar{r},\omega)|^2\rangle = |V_{in}(\omega)X_t(\omega)X_r(\omega)|^2\cdot A_s(\bar{r},\omega)\cdot\xi^4\cdot\eta(\bar{r},\omega)\cdot l\cdot D_s(\bar{r},\omega), \quad (2)$$

where $V_s(\bar{r},\omega)$ is the received voltage signal from the scattering volume, $\eta(\omega)$ the backscatter coefficient, l the length of the gate, $D_s(\bar{r},\omega)$ the mean diffraction correction coefficient, $V_{in}(\omega)$, $X_t(\omega)$ and $X_r(\omega)$ represent the electrical signal driving the transducer and the electromechanical coupling factor of the transducer in transmit and receive mode, respectively, ξ^4 the transmission loss through the medium-tissue interface and A_s the function describing the total attenuation effects.

The ratio of the power spectra from the distal and proximal windows can be expressed as

$$\frac{\langle|V_s(r_d,\omega)|^2\rangle}{\langle|V_s(r_p,\omega)|^2\rangle} = \frac{A_s(r_d,\omega)\cdot D_s(r_d,\omega)\cdot\eta(r_d,\omega)}{A_s(r_p,\omega)\cdot D_s(r_p,\omega)\cdot\eta(r_p,\omega)}, \quad (3)$$

where the subscripts d and p represent the distal and proximal window of the data block, respectively. By making the assumption that the effective size of the scatterers is constant so that the BSC varies in the form $\eta(r_p,\omega) = c\cdot\eta(r_d,\omega)$, Eq. (2) can be arranged as

$$\frac{c\cdot A_s(r_p,\omega)}{A_s(r_d,\omega)} = \frac{\langle|V_s(r_p,\omega)|^2\rangle}{\langle|V_s(r_d,\omega)|^2\rangle}\cdot\frac{D_s(r_d,\omega)}{D_s(r_p,\omega)}, \quad (4)$$

The ratio between the distal and proximal window attenuation functions can be written as

$$\frac{A_s(r_p,\omega)}{A_s(r_d,\omega)} = \frac{\exp(-4\alpha(\omega)\cdot(r_p-r_0))\cdot A_c(r_0,\omega)}{\exp(-4\alpha(\omega)\cdot(r_d-r_0))\cdot A_c(r_0,\omega)}, \quad (5)$$

where A_c is the cumulative attenuation function from the transducer to the initial depth r_0 of the data block. Replacing (5) in (4) and applying natural logarithm to both sides of the equation results in

$$\ln\left[\frac{c\cdot\exp(-4\alpha(\omega)\cdot r_d)}{\exp(-4\alpha(\omega)\cdot r_p)}\right] = \ln\left[\frac{\langle|V_s(r_p,\omega)|^2\rangle}{\langle|V_s(r_d,\omega)|^2\rangle}\cdot\frac{D_s(r_d,\omega)}{D_s(r_p,\omega)}\right]. \quad (6)$$

The attenuation coefficient slope γ can be obtained by performing a linear fit to the right side of (5), i.e.,

$$\alpha(\omega)+\frac{\ln c}{4\cdot(r_d-r_p)} = \frac{1}{4\cdot(r_d-r_p)}\cdot\ln\left[\frac{\langle|V_s(r_p,\omega)|^2\rangle}{\langle|V_s(r_d,\omega)|^2\rangle}\cdot\frac{D_s(r_d,\omega)}{D_s(r_p,\omega)}\right]. \quad (7)$$

Finally, the attenuation coefficient slope β in dB/cm-MHz can be calculated as

$$\beta = 8.6858\gamma \quad (8)$$

D. Statistics:

For statistics, manual segmentation using custom MATLAB software of the data blocks that were fully included on each thyroid lobes was performed. To ensure an unbiased data processing, the operator was not aware of the histopathological reports. Attenuation coefficient slope images were constructed by averaging data from three adjacent slices in order to reduce estimate variance. Outliers in the data were previously omitted automatically using the modified Thompson's Tau method relying on the sample's standard deviation.

Finally, due to the relatively small size of the population, a non-parametric Kruskal-Wallis test was conducted among each group to detect significant differences between the histopathological groups of study.

III. Experimental Results

Examples of the B-mode images obtained from normal, PTC, FV-PTC and C-cell diseased thyroids are shown in the left column of Fig. 2. Although the gross shape of the thyroids can help to differentiate between normal and diseased cases, classification using conventional ultrasonic imaging is not evident. The corresponding attenuation coefficient slope images are shown in the right column of Fig. 2. The differences between the attenuation estimate maps of the c-Cell adenoma sample and the other groups (right column of Fig.2) are clearly visible now. Moreover, the mean attenuation coefficient slope value in the C-cell sample is noticeably higher.

Fig. 3 shows the distribution of the mean attenuation coefficient slope for all animals considered in this study. The estimated values for the complete mice model varies from 0.92 to 1.68 dB/(MHz·cm) and the mean value is 1.32 ± 0.20 dB/cm-MHz. The scatter plot shows that all the c-Cell group mean attenuation values are over the 1.5 dB/cm-MHz threshold. On the other hand the mean attenuation values of the control group and the other two pathologies are distributed under this value.

The Kruskal-Wallis box plot report is presented in Fig. 4. The median and interquartile range for each group were 1.29 and 0.22 dB/cm-MHz for the control group, 1.64 and 0.09 dB/cm-MHz for c-Cell, 1.16 and 0.12 dB/cm-MHz for PTC and 1.33 and 0.08 dB/cm-MHz for FV-PTC, respectively. The two malignant groups reported relatively high p-values when compared to the control group (p= 0.18 and 0.2453). However, when comparing both malignant groups against each other (p=0.0176) evidence of independence between groups was demonstrated. Furthermore, results reported statistically significant differences between the c-Cell group and the other groups of study (p = 0.009, 0.0034 and 0.0062 for FV-PTC, PTC and control groups respectively).

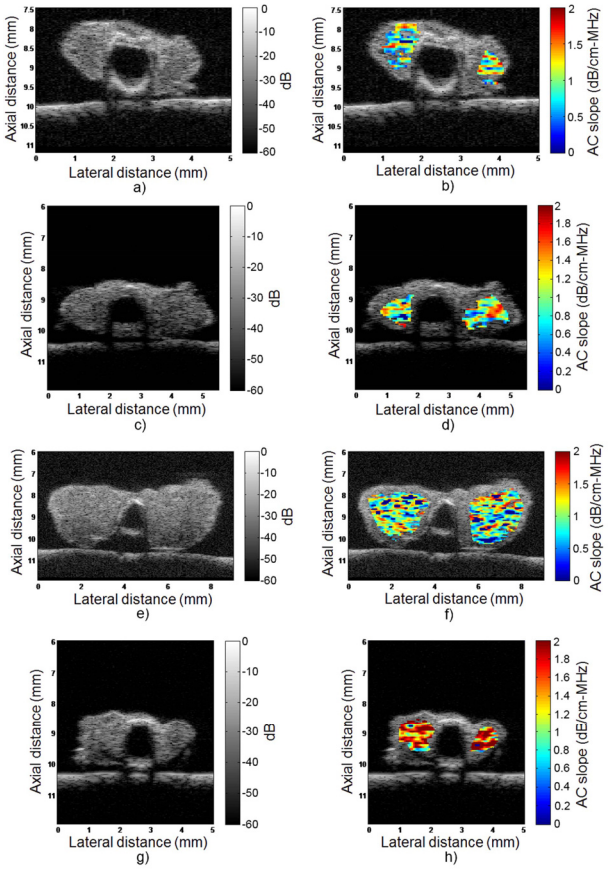

Fig. 2. a), c), e) and g) B-mode and b) ,d) ,f) and h) Quantitative ultrasound attenuation coefficient slope enhanced images of a control, FV-PTC, PTC and C-cell adenoma thyroid respectively.

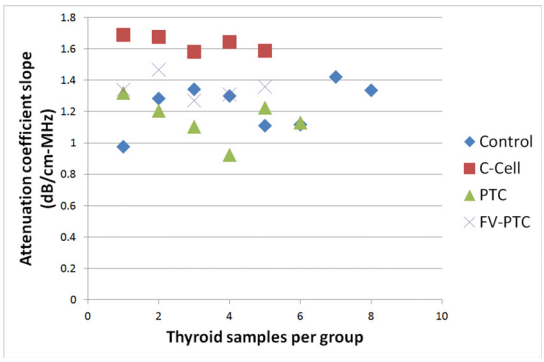

Fig. 3. Mean attenuation coefficient slope value distribution of the thyroids used in this study.

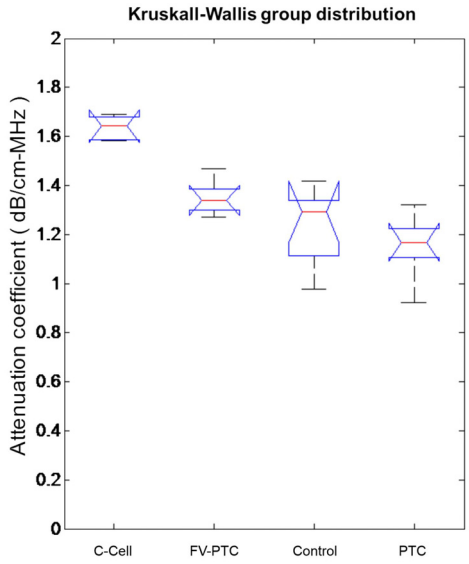

Fig. 4. The Kruskal-Wallis group distribution of the thyroids used in this study.

IV. Discussion

The estimated mean values are consistent with values obtained previously by an insertion loss method which obtained a mean attenuation value of the sample of 1.19 ± 0.26 dB/cm-MHz [4] in mice thyroids. These values are also consistent with reports of attenuation in human thyroids [11].

A high-frequency transducer (45 MHz) was required due to the small size of the mouse thyroids and the need of sufficient samples on each RF-line. This frequency is not normally available for clinical ultrasound. However, due to the larger size of a human thyroid, ultrasound signals at the higher end of the clinical ultrasound frequencies (~ 20 MHz) should be explored to assess the reproducibility of these findings on humans.

In previous studies, the FV-PTC and PTC groups in mouse models were identified using ESD and EAC [4,10]. However, these estimators could not differentiate the C-cell adenomas from the normal thyroids. Based on the results of the present study, the use of AC and BSC estimates in conjunction could completely characterize the four sample groups under examination.

V. Conclusion

The experimental results suggest that quantitative ultrasonic attenuation imaging can potentially discriminate C-cell adenomas on thyroid tissues from malignant and normal tissues ($p<0.05$) and between different malignant cases (i.e., PTC and FV-PTC, $p<0.05$). The use of attenuation coefficient slope estimates in conjunction with other quantitative ultrasound parameters (i.e., ESD and EAC) would potentially allow detecting and differentiating malignant and benign lesions from normal tissue.

Acknowledgment

The authors would like to thank Rita Miller and Emily Hartman for their assistance in scanning and animal handling. This work was supported by NIH Grant R21-CA139095 and PUCP Grants DGI 2012-0149 and 2013-0131.

References

[1] L. Morris, A. Sikora, T. Tosteson and L. Davies, "The increasing incidence of thyroid cancer: the influence of access to care," *Thyroid*, vol. 23, pp.885-891, July 2013.

[2] C. Cappelli et.al. "The predictive value of ultrasound findings in the management of thyroid nodules," *QJM: An International Journal of Medicine*, vol. 100, pp.29-35, January 2007.

[3] L. Davies, M.Ouellette, M.Hunter and G.Welch. "The increasing incidence of small thyroid cancers: Where are the cases coming from?," *Laryngoscope*, vol. 120, pp.2446-2450, December 2010.

[4] R. Lavarello, W. Ridgway, S. Sarwate and M. Oelze, "Characterization of thyroid cancer in mouse models using high-frequency quantitative ultrasound techniques," Ultrasound in Medicine & Biology, accepted for publication, 2013.

[5] Y. Labyed and T. Bigelow, "A theoretical comparison of attenuation measurement techniques from backscattered ultrasound echoes," *Journal of the Acoustical Society of America*, vol. 129, pp. 2316-2324, April 2011.

[6] H. Kim and T. Varghese, "Hybrid spectral domain method for attenuation slope estimation," *Ultrasound in Medicine & Biology*, vol. 34, pp. 1808–1819, November 2008.

[7] H. Kim and T. Varghese, "Attenuation estimation using spectral cross-correlation," *IEEE Transactions on Ultrasonics, Ferroelectrics and Frequency Control*, vol. 54, pp.510-520, March 2007.

[8] X.Chen, D. Phillips, K. Schwarz, J. Mottley and K. Parker "The measurement of backscatter from a broadband pulse-echo system - A new formulation," *IEEE Transactions on Ultrasonics, Ferroelectrics and Frequency Control*, vol. 44, pp.515-526, March 1997.

[9] D. Panizo, G. Ghoshal, M. Oelze and R. Lavarello, "Accuracy of backscatter coefficient estimation using highly focused transducers," in *Proceedings of the IEEE International Ultrasonics Symposium*, pp. 2344 – 2347, 2012.

[10] R. Lavarello, B. Ridgway, S. Sarwate and M. Oelze, "Imaging of follicular variant papillary thyroid carcinoma in a rodent model using spectral-based quantitative ultrasound techniques," in *Proceedings of the IEEE International Symposium on Biomedical Imaging*, pp. 732-735, 2013.

[11] Y. Fujii, N. Taniguchi, K. Itoh and K. Omoto "Attenuation coefficient measurement in the thyroid," *Journal of Ultrasound in Medicine*, vol. 22, pp. 1067–1073, 2003.